

# Device-independent demonstration of genuine multipartite entanglement

Julio T. Barreiro<sup>\*a,1</sup>, Jean-Daniel Bancal<sup>\*b,2</sup>, Philipp Schindler,<sup>1</sup> Daniel Nigg,<sup>1</sup>

Markus Hennrich,<sup>1</sup> Thomas Monz,<sup>1</sup> Nicolas Gisin,<sup>2</sup> and Rainer Blatt<sup>1,3</sup>

<sup>1</sup>*Institut für Experimentalphysik, Universität Innsbruck, Technikerstrasse 25, 6020 Innsbruck, Austria*

<sup>2</sup>*Group of Applied Physics, University of Geneva, Geneva, Switzerland*

<sup>3</sup>*Institut für Quantenoptik und Quanteninformation, Österreichische Akademie der Wissenschaften, Technikerstrasse 21A, 6020 Innsbruck, Austria*

<sup>\*</sup> *These authors contributed equally to this work.*

Entanglement in a quantum system can be demonstrated experimentally by performing the measurements prescribed by an appropriate entanglement witness [1]. However, the unavoidable mismatch between the implementation of measurements in practical devices and their precise theoretical modelling generally results in the undesired possibility of false-positive entanglement detection [2]. Such scenarios can be avoided by using the recently developed device-independent entanglement witnesses (DIEWs) for genuine multipartite entanglement [3]. Similarly to Bell inequalities, DIEWs only assume that consistent measurements are performed locally on each subsystem. No precise description of the measurement devices is required. Here we report an experimental test of DIEWs on up to six entangled  $^{40}\text{Ca}^+$  ions. We also demonstrate genuine multipartite quantum nonlocality between up to six parties with the detection loophole closed.

Entanglement enables many quantum tasks, including scalable quantum communication [4], secure quantum key distribution [5, 6] and quantum computing [7]. Entanglement thus represents a key resource for quantum information processing. As the experimental systems developed to host and manipulate entangled states diversify [8–11], clear tests are desired that are able to certify properly the entanglement of such states. In particular, tests of genuine multipartite entanglement are needed to show that the entanglement truly involves all of their constituents [1].

Tools to detect genuine multipartite entanglement have been developed [1] and used to demonstrate, for instance, entanglement between up to 8-10 photonic qubits [12, 13] or 14 ions [14]. Namely, it was shown that every multipartite entangled state can be detected by a hermitian operator known as an entanglement witness, whose expectation value is negative on the considered state but positive on all biseparable states. Any measurement of a witness yielding a negative value thus certifies that the measured state is multipartite entangled. Experimentally speaking, entanglement witnesses are convenient because they can be expressed in terms of simple measurable observables specific to the physical system, in contrast to joint measurements over multiple copies.

Although entanglement witnesses are very well understood from a theoretical point of view, their application to practical systems strongly relies on the way that concrete systems are modeled. For example, entanglement witnesses generally take different forms depending

on the dimension of the Hilbert space under consideration. An artificial truncation of this space can thus lead to wrong entanglement detection (e.g., in photon number [15]). Similarly, any mismatch between the measurements prescribed and those performed, such as systematic errors, can also lead to flawed entanglement detection [2]. Entanglement witnesses can also be evaluated on a state reconstructed by tomography [16, 17], but the reconstruction also relies on a detailed model of the measurement devices and Hilbert space dimensionality (see e.g. Ref. [18] for possible consequences of using a wrong model). In particular, quantum state tomography is also sensitive to systematic measurement errors [2].

Systematic errors and untenable assumptions may lead one to conclude that any proper experimental entanglement certification requires a particularly good prior knowledge of the measurement devices. But this is not the case: a rudimentary measurement model, whose validity can in principle be checked in practice, is sufficient to demonstrate entanglement properties of quantum systems. Namely, entanglement can be certified under the sole hypothesis that each subsystem can be addressed individually with independent measurement devices. Indeed, this condition allows one to ensure that, upon measurement of a separable quantum state, the raw statistics satisfy all Bell inequalities [1]. Violation of a Bell inequality under these conditions thus certifies that the measured state was entangled. In contrast with conventional entanglement witnesses, this conclusion holds independently of the internal mechanisms of the measurement devices used in the experiment [19] (device independently as in recent tests of classical and quantum dimensions [20–22]). Because Bell inequalities, in general, do not detect genuine multipartite entanglement, dedicated device-independent witnesses were recently developed in the form of DIEWs [3, 23, 24].

<sup>a</sup> Present address: Fakultät für Physik, Ludwig-Maximilians-Universität München & Max-Planck Institute of Quantum Optics, Germany

<sup>b</sup> Present address: Centre for Quantum Technologies, National University of Singapore, Singapore

Several architectures have realized multi-particle entanglement [8–11] but trapped ions have demonstrated particularly high fidelity in the preparation, manipulation and detection of quantum states. Similar to other systems, however, such ion trap architectures are affected by crosstalk. This imperfection occurs on systems in which measurements or operations intended on individual qubits affect neighboring qubits (close physically or in frequency, for example). Because crosstalks were not considered in the original derivation of DIEWs [3], we adapted the bound of the tested witnesses to take this imperfection into account. We then demonstrate genuine multipartite entanglement between three, four and six trapped ions with the aid of these DIEWs.

As described in detail in Ref. [3], let us consider an entangled state consisting of  $n$  parties or subsystems and a device-independent scenario where the measurement settings and outcomes are only referred to by indices and without alluding to the specifics of how these measurements are performed. We consider that a party  $j$  of this state is measured in one of  $m$  possible ways. We thus index this measurement setting by  $s_j = 0, \dots, m-1$ . We also consider that the local measurement of each party yields one of two outcomes that we index by  $r_j = 0, 1$ . We can thus identify a measurement on the entire  $n$ -partite system by the vector  $\vec{s} = (s_1, \dots, s_n) \in \{0, \dots, m-1\}^n$ . Similarly, we describe each possible outcome of a measurement on the entire system by a vector  $\vec{r} = (r_1, \dots, r_n) \in \{0, 1\}^n$ . After measuring the state, the conditional probability, or raw statistics, of observing the outcome  $\vec{r}$  given that the choice of measurement settings  $\vec{s}$  is applied to each of the  $n$  qubits is denoted by  $P(\vec{r}|\vec{s})$ . For an  $n$ -partite state with the described measurements and outcomes, we define the DIEW parameter as

$$I_{nm} = \sum_{s \equiv 0 \pmod{m}} (-1)^{s/m} E_{\vec{s}} + \sum_{s \equiv 1 \pmod{m}} (-1)^{(s-1)/m} E_{\vec{s}} \quad (1)$$

where  $E_{\vec{s}} = \sum_{\vec{r}} (-1)^r P(\vec{r}|\vec{s})$  is the  $n$ -partite correlator;  $s = \sum_j s_j$  and  $r = \sum_j r_j$  (see Ref. [24]).

As shown in Ref. [24], because all biseparable quantum correlations satisfy

$$I_{nm} \leq 2m^{n-2} \cot(\pi/2m) \equiv B_{nm},$$

this inequality can be used as a DIEW to detect *genuine  $n$ -partite entanglement*. In contrast with usual entanglement witnesses,  $I_{nm}$  provides no explicit description of the observables to be measured on each subsystem. Yet, every practical evaluation of Eq. (1) is necessarily performed with some measurement operators  $M_{r_j|s_j}^j$  so that the observed correlations can be written as

$P(\vec{r}|\vec{s}) = \text{Tr} \left[ \bigotimes_{j=1}^n M_{r_j|s_j}^j \rho \right]$ . Here  $M_{r_j|s_j}^j$  is the measurement operator acting locally on subsystem  $j$  corresponding to setting  $s_j$  and outcome  $r_j$ , and  $\rho$  is the measured quantum state. The DIEW parameter can thus be understood as the expectation value of a quantum operator  $\mathcal{I}_{nm}$  whose biseparable bound is given by  $B_{nm}$  (see Supplementary Information for a definition of  $\mathcal{I}_{nm}$ ). In particular, the quantity  $\mathcal{W}_{nm} = B_{nm}\mathbb{1} - \mathcal{I}_{nm}$  is a standard entanglement witness for genuine multipartite entanglement [1]. Therefore, any practical evaluation of a DIEW amounts to test a standard witness that is adapted to the measurement operators available during the experiment. In addition, DIEWs need less measurements and data processing than complete state tomography (see Methods).

We focus on a class of multipartite states routinely prepared in our experiment, the genuinely entangled  $n$ -qubit state  $|GHZ\rangle_n = \frac{1}{\sqrt{2}}(|0\rangle^{\otimes n} + |1\rangle^{\otimes n})$  which yields the maximum value of our DIEW parameter

$$I_{nm}^{max} = 2m^{n-1} \cos(\pi/2m) > B_{nm}$$

when the following  $m$  measurements act on each qubit  $j$  in the  $x$ - $y$  plane of the Bloch sphere

$$\cos(\phi_{s_j})\sigma_x^{(j)} + \sin(\phi_{s_j})\sigma_y^{(j)}, \quad \text{with} \quad \phi_{s_j} = -\frac{\pi}{2mn} + s_j \frac{\pi}{m} \quad \text{for } s_j = 0, \dots, m-1, \quad (2)$$

where  $\sigma_{x,y,z}^{(j)}$  are the Pauli matrices for qubit  $j$  (see Supplementary Information for the optimization procedure). For a given measurement  $\vec{s}$  on all qubits, this measurement setting is then equivalent to rotating each qubit with  $\exp(-i\frac{\phi_{s_j}}{2}\sigma_z^{(j)})$  for every  $j$ , followed by a collective rotation of all qubits with  $\exp(-i\frac{\theta}{2}\sum_j \sigma_x^{(j)})$  where  $\theta = \pi/2$ , and a measurement in the computational basis. Our witness is indeed device-independent: if these operations are not implemented as expected, because the  $\phi_{s_j}$  take unprescribed values, or  $\theta \neq \pi/2$ , and consequently the measurement operators  $M_{r_j|s_j}^j$  change, then by construction [3] the bound  $I_{nm} \leq B_{nm}$  still holds for all biseparable states whatever the actual measurement operators  $M_{r_j|s_j}^j$  are, thus avoiding false positive entanglement detection.

In the experiment each qubit was encoded in the internal electronic Zeeman levels  $4S_{1/2}(m = -1/2) = |1\rangle$  and  $3D_{5/2}(m = -1/2) = |0\rangle$  of a  $^{40}\text{Ca}^+$  ion. Three, four or six ions were confined to a string by a linear Paul trap and cooled to the ground state of the axial center-of-mass mode [25]. The entanglement among qubits was realized through a Mølmer-Sørensen [26, 27] entangling operation using a bichromatic light field collectively illuminating all ions [14] [e.g., Fig. 1a]. Single-qubit rotations  $\exp(-i\frac{\phi_j}{2}\sigma_z^{(j)})$  were driven by a far off-resonantly

detuned laser pulse focused on the target ion  $j$  and inducing an AC-Stark effect, where  $\phi_j$  is determined by the detuning and the pulse duration [e.g., Fig. 1b]. Collective qubit rotations  $\exp(-i\frac{\theta}{2}\sum_j\sigma_x^{(j)})$  were driven by a laser pulse exciting the qubit transition, where  $\theta$  is given by the Rabi frequency of the qubits and the duration of the pulse [e.g., Fig. 1c]. At the end the qubits were measured in the computational basis through an electron-shelving technique scattering light on the dipole transition  $4S_{1/2} \leftrightarrow 4P_{1/2}$ . The scattered light was detected with a CCD camera that resolves each ion's fluorescence.

In this setup, the subsystems may indeed leave the qubit subspace, albeit with an expected very small probability, during initialization, preparation and measurement of the entangled state (see Methods). Using a DIEW allows us to discard these considerations safely.

In practice we observe that applying a qubit rotation on an ion produces an unintended rotation on neighboring ions (see Fig. 1b and Methods). Because this crosstalk effect is not included in the device-independent framework, which assumes all measurements to be defined locally, we analysed the impact that these crosstalks can have on the bound  $B_{nm}$ . For simplicity, however, we only considered a crosstalk upper bound  $\epsilon$ . In our system we found that  $\epsilon = \{1.6, 5, 4\}\% \pm \{0.1, 1, 1\}\%$  for  $\{3, 4, 6\}$  ions. We then computed numerically the maximum impact  $\Delta I^{CT} = I_{bisep}^\epsilon - I_{bisep}^{\epsilon=0}$  that crosstalks bounded by  $\epsilon$  can have on the biseparable bound for the settings intended for the experiment ( $CT$  stands for crosstalks). Assuming that the maximum contribution of the crosstalks to Eq. 1 is given by  $\Delta I^{CT}$ , we update the bound to  $B_{nm}^{CT} = B_{nm} + \Delta I^{CT}$ .

With three ions, we performed a DIEW measurement on a state prepared towards  $|GHZ\rangle_3$  as described above. For the  $m=2(3)$  settings DIEW of Eq. 2 each measurement set consists of 8 (18) measurements. To acquire significant statistics, we performed 6 (264) measurement sets where each measurement was done on 250 consecutive copies of the state (Table I). For each set the order of the measurements was chosen randomly in order to avoid correlations between outcomes and unaccounted changes or drifts on the experimental conditions.

To demonstrate genuine four- and six-partite entanglement with DIEWs, we avoided a decay of coherence, quadratic in the number of qubits [14] (see Methods), by preparing the decoherence-free GHZ states  $\frac{1}{\sqrt{2}}(|0011\rangle + |1100\rangle)$  and  $\frac{1}{\sqrt{2}}(|000111\rangle + |111000\rangle)$ . These states have a coherence time of  $\approx 300$  ms, sufficient for our measurements. For a DIEW measurement of Eq. 2, the angles  $\phi_{s_j}$  that maximize the violation for these states depend on the number of settings  $m$  and the number of qubits  $n$  (see Supplementary Information). For  $m = 2$  settings ( $s_j = 0, 1$ ), a maximum violation is achieved when one half of the qubits is measured with an angle  $\phi_{s_j} = s_j\frac{\pi}{2}$  and the other half with  $\phi'_{s_j} = \frac{n+1}{12n}\pi + \frac{1-s_j}{2}\pi$ .

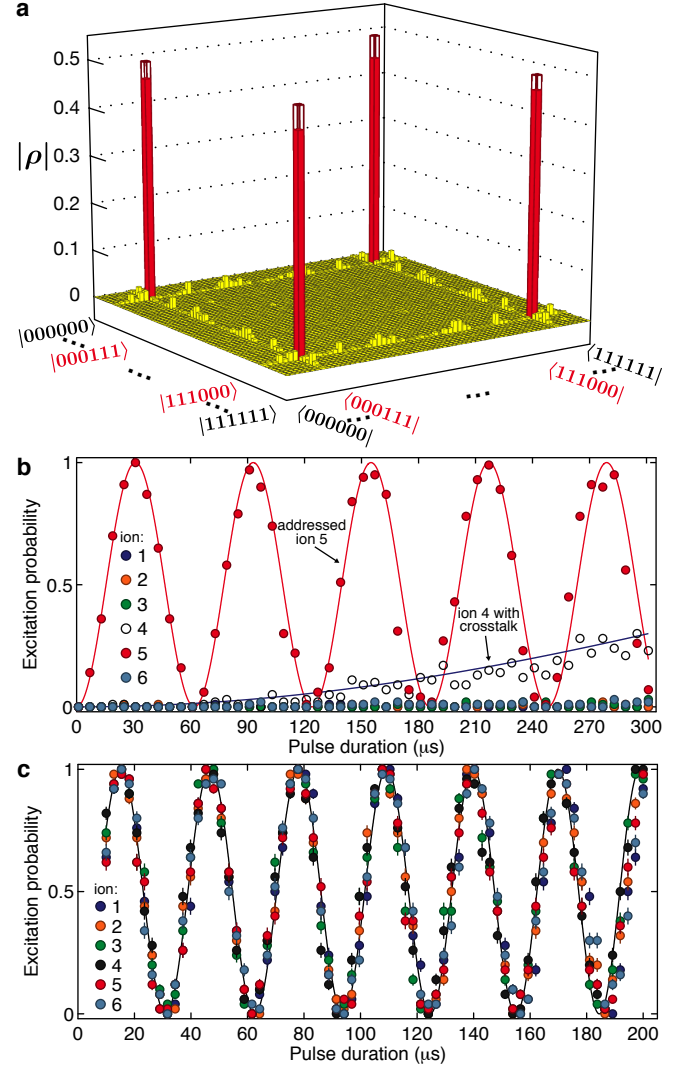


**Figure 1. State and measurement characterization for the six-qubit DIEW measurement.** **a**, Reconstructed density matrix  $\rho$  (absolute value) of six-qubit state  $\sim |000111\rangle + e^{i\pi/2}|111000\rangle$ . The reconstructed state has a fidelity of 91.9(3)% with the target state. **b**, Single-qubit excitations while driving a single-qubit rotation of the fifth qubit (red markers) on a six-ion string, in this case, the crosstalk, due to imperfect focusing, is biggest for the fourth ion (black open circle markers). The red line corresponds to a sinusoidal fit to the excitation of the fifth ion, and the black line to the fourth ion. The corresponding fits to the excitation of ions 1, 2, 3 and 6 (markers dark blue, orange, green, and light blue) are not shown as the respective excitations are negligible. **c**, Single-qubit excitations during a six-qubit collective rotation. All ions are homogeneously excited as the pulse duration is increased. The sinusoidal fit, shown as a black line, is done for all points. Error bars are  $1\sigma$  where shown, otherwise smaller than the marker.

For  $m = 3$  settings ( $s_j = 0, 1, 2$ ), the corresponding angles are  $\phi_{s_j} = \frac{n+1}{12n}\pi + s_j\frac{\pi}{3}$  and  $\phi'_{s_j} = \frac{2-s_j}{3}\pi$ . The measured DIEW parameters shown in Table I significantly violate the thresholds for genuine four- and six-partite

TABLE I. Summary of DIEW measurements with  $n = 3, 4, 6$  qubits and  $m = 2, 3$  settings.<sup>a</sup>

$n$	$m$	$B$	$B^{CT}$	$I^{exp}$	$I^{exp} - B^{CT} (\sigma)$	$I^{max}$	$V = I^{exp}/I^{max}$	$q$ (%)	copies/meas.	meas./set	sets	copies
3	2	4	4.070(4)	4.78(6)	12	$4\sqrt{2}$	0.84(1)	15(1)	250	8	6	12k
	3	$6\sqrt{3}$	10.542(9)	12.39(1)	136	$9\sqrt{3}$	0.7948(9)	14.9(1)	250	18	264	1188k
4	2	8	8.43(8)	10.42(6)	20	$8\sqrt{2}$	0.92(1)	19(1)	50	16	60	48k
	3	$18\sqrt{3}$	32.5(2)	42.53(8)	41	$27\sqrt{3}$	0.909(7)	23.7(6)	50	54	60	162k
6	2	32	34.0(5)	40(1)	5	$32\sqrt{2}$	0.88(3)	15(3)	5	64	21	6720
	3	$162\sqrt{3}$	294(3)	374(3)	19	$243\sqrt{3}$	0.89(1)	21(1)	5	486	21	51030

<sup>a</sup> Errors in parenthesis,  $1\sigma$ , were derived from propagated statistics in the measured expectation values with 1000 Monte Carlo samples.  $B$ : biseparable quantum correlations bound,  $B^{CT}$ : updated  $B$  to account for crosstalks,  $I^{exp}$ : measured DIEW,  $I^{max}$ : quantum DIEW bound,  $V$ : visibility,  $q = (I^{exp} - B^{CT})/I^{exp}$ : maximum admissible additional white noise. The magnitude of the violation,  $I^{exp} - B^{CT}$ , is given in units of  $\sigma$  (gray column).

TABLE II. Comparison of DIEW measurements with  $m = 2$  and  $m = 3$  settings for a similar number of copies of the state of  $n = 3, 4$ , and  $6$  qubits.<sup>a</sup>

$n$	$m$	$I^{exp}$	$I^{exp} - B^{CT} (\sigma)$	$q$ (%)	copies
3	2	4.67(9)	7	13(2)	4800
	3	12.2(2)	8	14(2)	4752
4	2	10.5(2)	10	20(2)	3840
	3	41.7(6)	14	22(2)	3240
6	2	41(1)	6	17(3)	1344
	3	376(6)	12	22(2)	1458

<sup>a</sup> Errors in parenthesis,  $1\sigma$ , were derived from propagated statistics in the measured expectation values with 1000 Monte Carlo samples.  $B^{CT}$ : updated biseparable quantum correlations bound to account for crosstalks,  $I^{exp}$ : measured DIEW,  $q = (I^{exp} - B^{CT})/I^{exp}$ : maximum admissible additional white noise. The magnitude of the violation,  $I^{exp} - B^{CT}$ , is given in units of  $\sigma$  (gray column).

entanglement.

To compare the two- and three-settings DIEW measurements with the same number of copies, we chose random subsets of copies from each measurement of the above data. The results in Table II show a higher violation for the three settings measurements with four and six ions. This indicates that the detection of entanglement through our witness is made easier by using more settings. Moreover, the maximum amount of white noise  $q$  that can be mixed with the observed statistics before losing the violation indicates that more states are detected by the 3-settings than the 2-settings DIEW (see also Table I).

Because DIEW inequalities with  $m = 2$  settings are equivalent to  $n$ -partite Svetlichny inequalities [28, 29], they detect not only multipartite entanglement but also multipartite quantum nonlocality [3]. However, for  $m \geq 3$  settings, the DIEW inequalities are not Svetlichny inequalities: Svetlichny inequalities witness both, multipartite entanglement and quantum nonlocality, but DIEW inequalities, in general, only witness multipartite entanglement (multipartite entanglement is necessary in order to show multipartite quantum nonlocality) [3]. Multipartite entanglement can thus be detected device-independently even when no Svetlichny inequality

can be violated. This is indicated by the results of Table II for  $n = 6$ : For some amount of additional noise, the violation of the 2-settings inequality disappears while the 3-settings inequality can still be violated. Note that violation of a three-partite Svetlichny inequality was previously demonstrated with photons in absence of crosstalks [30], but leaving the locality and detection loopholes open.

With today's technology, the different parts of an entangled system cannot always be well separated from each other. However, clear separation of the parts is certainly a desired feature in the long term, since it is necessary to take full advantage of quantum entanglement. As shown above, entanglement can be demonstrated in these circumstances without relying on a precise description of the measurement devices used, a knowledge which is never available completely. The achieved demonstration was thus more robust than conventional entanglement demonstrations and nevertheless simple. In order to guarantee the absence of crosstalks, we look forward to a demonstration with clearer separation between the parties or closing the locality loophole. On the theoretical side, further work is needed to conceive device-independent tests of resource states sufficient for interesting quantum simulation or communication protocols.

**Acknowledgments** We thank Y.-C. Liang for useful discussions. We gratefully acknowledge support by the Austrian Science Fund (FWF) through the SFB FoQuS (FWF Project No. F4006-N16) and by the Swiss NCCR Quantum Science and Technology, the CHIST-ERA DIQIP, and the European ERC-AG QORE.

## METHODS SUMMARY

**DIEW and tomography.** For  $n$  parties and  $m$  possible measurement settings per party, the total number of measurements settings required for the witness in Eq. (1) is  $2m^{n-1}$  whereas tomography requires  $(d^2 - 1)^n$  measurements, where  $d$  is the dimension of each party or subsystem [1]. For  $m = 3$  and qubits ( $d = 2$ ), for example, this witness requires two thirds the number of measurements required for full quantum state tomography (this advan-

tage becomes more evident as the dimension of the system increases). In addition, the required post-processing is trivial in comparison with state reconstruction methods. Naturally, considering  $m = 2$  gives the minimum total number of measurements required, but as shown in the main text, considering  $m = 3$  should result in more robust violations. For  $m = 4$  and  $d = 2$ , however, the DIEW measurement requires more measurements than tomography.

**Experimental leak of qubit subspace.** The qubits are initialized into the state  $4S_{1/2}(m_j = -1/2) = |1\rangle$  with a 99.9% probability, with the remaining population in the  $4S_{1/2}(m_j = +1/2)$ . Also, during the entangling operation, the motional ground state can be unintentionally abandoned for higher motional states. Furthermore, our state detection protocol identifies as population in the state  $|1\rangle$  any observation of fluorescence on the dipole transition, including  $4S_{1/2}(m_j = -1/2)$  and higher vibrational states.

**Experimental crosstalks.** In practice we observe that applying the rotation  $\exp(-i\frac{\varphi_j}{2}\sigma_z^{(j)})$  on ion  $j$  produces an unintended rotation  $\varphi_k$  on qubit  $k$  because of residual light from imperfect focusing [25] (e.g., Fig. 1b). This imperfection affects the net rotation applied on ion  $k$ , so that the measurement applied on ion  $k$  depends slightly on the one applied on ion  $j$ . These crosstalks can be quantified by the matrix  $C_{jk} = \varphi_k/\varphi_j$ , and the operation intended only on ion  $j$  is then described by the operation on all ions  $\exp(-i\sum_k \frac{\varphi_j}{2} C_{jk} \sigma_z^{(k)})$ . For simplicity, we only considered a crosstalk upper bound  $\epsilon > C_{jk}$ .

**Collective decay of three-qubit state.** Although the measured DIEW parameters shown in Table I for  $n = 3$  parties do violate the threshold for genuine three-partite entanglement, the observed visibilities of about 80% are incompatible with the 97% fidelity reported earlier [14]. This disagreement is due to the collective decay of the state during the DIEW measurement. Although the single-qubit coherence time in this experiment was  $\approx 10$  ms, the coherence time of the state  $|GHZ\rangle_3$  was only  $\approx 2$  ms. Because each single-qubit rotation took  $\approx 100 \mu\text{s}$  for a  $2\pi$  rotation (for collective rotations  $\approx 20 \mu\text{s}/2\pi$ ), and for each measurement the qubits were rotated sequentially, the state was significantly decaying during the DIEW measurement.

---

[1] Gühne, O. & Tóth, G. Entanglement detection. *Phys. Rep.* **474**, 1–75 (2009).  
 [2] Rosset, D., Ferretti-Schöbitz, R., Bancal, J.-D., Gisin, N. & Liang, Y.-C. Imperfect measurements settings: implications on quantum state tomography and entanglement witnesses. *arXiv:12030911* (2012).  
 [3] Bancal, J.-D., Gisin, N., Liang, Y.-C. & Pironio, S. Device-Independent Witnesses of Genuine Multipartite Entanglement. *Phys. Rev. Lett.* **106**, 250404 (2011).

[4] Briegel, H. J., Dür, W., Cirac, J. & Zoller, P. Quantum Repeaters: The Role of Imperfect Local Operations in Quantum Communication. *Phys. Rev. Lett.* **81**, 5932–5935 (1998).  
 [5] Ekert, A. K. Quantum cryptography based on Bell’s theorem. *Phys. Rev. Lett.* **67**, 661–663 (1991).  
 [6] Gisin, N., Ribordy, G., Tittel, W. & Zbinden, H. Quantum cryptography. *Rev. Mod. Phys.* **74**, 145–195 (2002).  
 [7] Briegel, H. J., Browne, D. E., Dür, W., Raussendorf, R. & Nest, M. V. d. Measurement-based quantum computation. *Nature Phys.* **5**, 19 (2009).  
 [8] DiCarlo, L. *et al.* Preparation and measurement of three-qubit entanglement in a superconducting circuit. *Nature* **467**, 574–578 (2010).  
 [9] Neumann, P. *et al.* Multipartite Entanglement Among Single Spins in Diamond. *Science* **320**, 1326–1329 (2008).  
 [10] Saffman, M., Walker, T. G. & Mølmer, K. Quantum information with Rydberg atoms. *Rev. Mod. Phys.* **82**, 2313–2363 (2010).  
 [11] Blatt, R. & Wineland, D. Entangled states of trapped atomic ions. *Nature* **453**, 1008–1015 (2008).  
 [12] Yao, X.-C. *et al.* Observation of eight-photon entanglement. *Nature Photon.* **6**, 225–228 (2012).  
 [13] Gao, W.-B. *et al.* Experimental demonstration of a hyper-entangled ten-qubit Schrödinger cat state. *Nature Phys.* **6**, 331–335 (2010).  
 [14] Monz, T. *et al.* 14-Qubit Entanglement: Creation and Coherence. *Phys. Rev. Lett.* **106**, 130506 (2011).  
 [15] Semenov, A. & Vogel, W. Fake violations of the quantum Bell-parameter bound. *Phys. Rev. A* **83**, 032119 (2011).  
 [16] Altepeter, J. B., James, D. F. V. & Kwiat, P. G. Qubit quantum state tomography. *Lecture Notes of Physics* **649**, 113–145 (2004).  
 [17] Lvovsky, A. I. Continuous-variable optical quantum-state tomography. *Rev. Mod. Phys.* **81**, 299–332 (2009).  
 [18] Audenaert, K. & Scheel, S. Quantum tomographic reconstruction with error bars: a Kalman filter approach. *New J. Phys.* **11**, 023028 (2009).  
 [19] Acín, A., Gisin, N. & Masanes, L. From Bell’s Theorem to Secure Quantum Key Distribution. *Phys. Rev. Lett.* **97**, 120405 (2006).  
 [20] Gallego, R., Brunner, N., Hadley, C. & Acín, A. Device-Independent Tests of Classical and Quantum Dimensions. *Phys. Rev. Lett.* **105**, 230501 (2010).  
 [21] Hendrych, M. *et al.* Experimental estimation of the dimension of classical and quantum systems. *Nature Phys.* **8**, 588–591 (2012).  
 [22] Ahrens, J., Badziag, P., Cabello, A. & Bourennane, M. Experimental device-independent tests of classical and quantum dimensions. *Nature Phys.* **8**, 592–595 (2012).  
 [23] Pál, K. & Vértesi, T. Multisetting Bell-type inequalities for detecting genuine multipartite entanglement. *Phys. Rev. A* **83**, 062123 (2011).  
 [24] Bancal, J.-D., Branciard, C., Brunner, N., Gisin, N. & Liang, Y.-C. A framework for the study of symmetric full-correlation Bell-like inequalities. *J. Phys. A: Math. Theor.* **45**, 125301 (2012).  
 [25] Schmidt-Kaler, F. *et al.* How to realize a universal quantum gate with trapped ions. *Appl. Phys. B: Lasers Opt.* **77**, 789–796 (2003).  
 [26] Mølmer, K. & Sørensen, A. Multiparticle Entanglement of Hot Trapped Ions. *Phys. Rev. Lett.* **82**, 1835–1838 (1999).  
 [27] Sackett, C. A. *et al.* Experimental entanglement of four

- particles. *Nature* **404**, 256–259 (2000).
- [28] Collins, D., Gisin, N., Popescu, S., Roberts, D. & Scarani, V. Bell-Type Inequalities to Detect True n-Body Nonseparability. *Phys. Rev. Lett.* **88**, 170405 (2002).
  - [29] Seevinck, M. & Svetlichny, G. Bell-Type Inequalities for Partial Separability in N-Particle Systems and Quantum Mechanical Violations. *Phys. Rev. Lett.* **89**, 060401 (2002).
  - [30] Lavoie, J., Kaltenbaek, R. & Resch, K. J. Experimental violation of Svetlichny’s inequality. *New J. Phys.* **11**, 073051 (2009).

# Device independent demonstration of genuine multipartite entanglement — SUPPLEMENTARY MATERIAL —

Julio T. Barreiro<sup>1\*</sup>, Jean-Daniel Bancal<sup>2\*</sup>, Philipp Schindler<sup>1</sup>, Daniel Nigg<sup>1</sup>,  
Markus Hennrich<sup>1</sup>, Thomas Monz<sup>1</sup>, Nicolas Gisin<sup>2</sup>, Rainer Blatt<sup>1,3</sup>

<sup>1</sup>Institut für Experimentalphysik, Universität Innsbruck, Technikerstr. 25, A-6020 Innsbruck, Austria

<sup>2</sup>Group of Applied Physics, University of Geneva, Geneva, Switzerland

<sup>3</sup>Institut für Quantenoptik und Quanteninformation, Österreichische Akademie der Wissenschaften,  
Technikerstr. 21A, A-6020 Innsbruck, Austria

\* These authors contributed equally to this work.

## CONTENTS

- I. Explicit example for the evaluation of the DIEW parameter  $I_{nm}$  1
- II. The DIEW parameter as the expectation value of the quantum operator  $\mathcal{I}_{nm}$  2
- III. Optimal measurement settings for the DIEW parameter  $I_{nm}$  2

## I. EXPLICIT EXAMPLE FOR THE EVALUATION OF THE DIEW PARAMETER $I_{nm}$

Here we show an explicit example of the terms involved on the DIEW parameter

$$I_{nm} = \sum_{s \equiv 0 \pmod{m}} (-1)^{s/m} E_{\vec{s}} + \sum_{s \equiv 1 \pmod{m}} (-1)^{(s-1)/m} E_{\vec{s}} \quad (1)$$

where  $E_{\vec{s}} = \sum_{\vec{r}} (-1)^r P(\vec{r}|\vec{s})$  is the  $n$ -partite correlator;  $s = \sum_j s_j$  and  $r = \sum_j r_j$  are the sums over all indices used in the measurement vector  $\vec{s}$  and the outcome vector  $\vec{r}$  (the colors will be evident in a moment). Obviously, for any settings  $\vec{s}$  the following is true  $\sum_{\vec{r}} P(\vec{r}|\vec{s}) = 1$ .

For  $n = 3$  qubits and  $m = 3$  measurement settings, there are  $3 \times 3 \times 3 = 27$  possible measurements as shown in the leftmost column in Table I. However, because the parameter  $I_{n=3,m=3}$  involves only those settings for which  $s \bmod 3$  is equal to 0 or 1, only 18 of the 27 measurement settings are necessary. These entries, involving  $s$  modulo 3 equal to 0 or 1, are shown in red and green font colors in Table I.

For our scenario where a measurement on each party has one of two possible outcomes, in our example with three parties, there are then eight possibilities, that is the vector of outcomes can take any of the following values:

$$\vec{r} \in \{\mathbf{000}, \mathbf{001}, \mathbf{010}, \mathbf{011}, \mathbf{100}, \mathbf{101}, \mathbf{110}, \mathbf{111}\},$$

where the vectors of possible outcomes are written here in boldface to distinguish them from the vector of measurement settings.

For example, when the vector of measurement settings is  $\vec{s} = (s_1, s_2, s_3) = (\mathbf{0}, \mathbf{1}, \mathbf{2})$ , then  $s = 3$  and  $s \equiv 0 \bmod 3$ , as shown in the row colored light gray in Table I. The 3-partite correlator term  $E_{012} = \sum_{\vec{r}} (-1)^r P(\vec{r}|\mathbf{012})$  is therefore involved in the parameter  $I_{33}$  as

$$\begin{aligned} (-1)^{(0+1+2)/3} E_{012} = & -[P(\mathbf{000}|\mathbf{012}) - P(\mathbf{001}|\mathbf{012}) \\ & + P(\mathbf{010}|\mathbf{012}) - P(\mathbf{011}|\mathbf{012}) \\ & + P(\mathbf{100}|\mathbf{012}) - P(\mathbf{101}|\mathbf{012}) \\ & + P(\mathbf{110}|\mathbf{012}) - P(\mathbf{111}|\mathbf{012})] \end{aligned}$$

In the scenario considered in which the measure-

TABLE I Measurement settings considered in the evaluation of the DIEW parameter  $I_{33}$ , see text.

$s_1$	$s_2$	$s_3$	$s$	$s \bmod 3$	$(-1)^{s/3}$	$(-1)^{(s-1)/3}$
0	0	0	0	0	1	
0	0	1	1	1		1
0	0	2	2	2		
0	1	0	1	1		1
0	1	1	2	2		
0	1	2	3	0	-1	
0	2	0	2	2		
0	2	1	3	0	-1	
0	2	2	4	1		-1
1	0	0	1	1		1
1	0	1	2	2		
1	0	2	3	0	-1	
1	1	0	2	2		
1	1	1	3	0	-1	
1	1	2	4	1		-1
1	2	0	3	0	-1	
1	2	1	4	1		-1
1	2	2	5	2		
2	0	0	2	2		
2	0	1	3	0	-1	
2	0	2	4	1		-1
2	1	0	3	0	-1	
2	1	1	4	1		-1
2	1	2	5	2		
2	2	0	4	1		-1
2	2	1	5	2		
2	2	2	6	0	1	

ments are prescribed by angles, the settings are  $\{\phi_{s_1}, \phi_{s_2}, \phi_{s_3}\} = \{\phi_0, \phi_1, \phi_2\}$ .

Another example, when  $\vec{s} = (s_1, s_2, s_3) = (2, 1, 1)$ , then  $s = 4$  and  $s \equiv 1 \pmod{3}$ , as shown in the row colored dark gray in Table I. The 3-partite correlator term  $E_{211} = \sum_{\vec{r}} (-1)^r P(\vec{r}|211)$  is therefore involved in the parameter  $I_{33}$  as

$$\begin{aligned} (-1)^{((2+1+1)-1)/3} E_{211} = & -[P(\mathbf{000}|211) - P(\mathbf{001}|211) \\ & + P(\mathbf{010}|211) - P(\mathbf{011}|211) \\ & + P(\mathbf{100}|211) - P(\mathbf{101}|211) \\ & + P(\mathbf{110}|211) - P(\mathbf{111}|211)] \end{aligned}$$

Again, in the scenario considered in which the measurements are prescribed by angles, the settings are  $\{\phi_{s_1}, \phi_{s_2}, \phi_{s_3}\} = \{\phi_2, \phi_1, \phi_1\}$ . For the 3-partite GHZ state, for example, the optimum angles calculated as described below, are

$$\begin{aligned} \phi_0 &= -\frac{\pi}{18} \\ \phi_1 &= -\frac{\pi}{18} + \frac{\pi}{3} \\ \phi_2 &= -\frac{\pi}{18} + \frac{2\pi}{3}. \end{aligned}$$

## II. THE DIEW PARAMETER AS THE EXPECTATION VALUE OF THE QUANTUM OPERATOR $\mathcal{I}_{nm}$

The value of  $I_{nm}$  can be understood as the expectation value of the operator  $\mathcal{I}_{nm}$  on the measured quantum state  $\rho$ , that is  $I_{nm} = \text{Tr}(\mathcal{I}_{nm}\rho)$ . From the definition of the parameter  $I_{nm}$  and the observed correlations  $P(\vec{r}|\vec{s}) = \text{Tr} \left[ \bigotimes_{j=1}^n M_{r_j|s_j}^j \rho \right]$ , the operator can naturally be written as

$$\begin{aligned} \mathcal{I}_{nm} &= \sum_{s \equiv 0 \pmod{m}} (-1)^{s/m} \sum_{\vec{r}} (-1)^r \bigotimes_{j=1}^n M_{r_j|s_j}^j + \\ & \sum_{s \equiv 1 \pmod{m}} (-1)^{(s-1)/m} \sum_{\vec{r}} (-1)^r \bigotimes_{j=1}^n M_{r_j|s_j}^j \\ &= \sum_{s \equiv 0 \pmod{m}} \sum_{\vec{r}} (-1)^{r+s/m} \bigotimes_{j=1}^n M_{r_j|s_j}^j + \\ & \sum_{s \equiv 1 \pmod{m}} \sum_{\vec{r}} (-1)^{r+(s-1)/m} \bigotimes_{j=1}^n M_{r_j|s_j}^j \end{aligned}$$

where  $M_{r_j|s_j}^j$  is the measurement operator acting locally on subsystem  $j$  corresponding to setting  $s_j$  and outcome  $r_j$ .

## III. OPTIMAL MEASUREMENT SETTINGS FOR THE DIEW PARAMETER $I_{nm}$

For every quantum state  $\rho$ , the measurement settings that yield the largest value of  $I_{nm}$  can be determined by

numerical optimization. In general, this can be achieved by parametrizing the measurement settings  $M_{r_j|s_j}^j$  of each party  $j$  inside their respective Hilbert space  $\mathcal{H}^j$  with a finite number of real variables. Gathering these variables for the measurement settings of all parties in a vector of parameters  $\vec{\alpha}$  then allows one to express the value of  $I_{nm}$  as a function of  $\vec{\alpha}$  only, by letting  $P(\vec{r}|\vec{s}) = \text{Tr}(\bigotimes_{j=1}^n M_{r_j|s_j}^j(\vec{\alpha}) \rho)$  in equation (1). The optimal settings are then given by  $M_{r_j|s_j}^j(\vec{\alpha}^*)$  where  $\vec{\alpha}^* = \arg \max I_{nm}(\vec{\alpha})$ .

In the case that the tripartite expression with  $m = 3$  settings  $I_{3,3}$  is evaluated on a GHZ state

$$|GHZ\rangle = \frac{1}{\sqrt{2}}(|000\rangle + |111\rangle),$$

for instance, the measurement operators corresponding to setting  $s_j$  of party  $j$  can be written as:

$$M_{0|s_j}^j = \frac{\mathbb{1} + \vec{n} \cdot \vec{\sigma}}{2}, \quad M_{1|s_j}^j = \mathbb{1} - M_{0|s_j}^j, \quad (2)$$

where  $\|\vec{n}\| = 1$  and  $\vec{\sigma} = (\sigma_x, \sigma_y, \sigma_z)$  is the vector of Pauli matrices. They can thus be parametrized by two real numbers  $\vartheta_{s_j}^j$  and  $\varphi_{s_j}^j$  by letting:

$$\vec{n} = \begin{pmatrix} \sin(\vartheta_{s_j}^j) \cos(\varphi_{s_j}^j) \\ \sin(\vartheta_{s_j}^j) \sin(\varphi_{s_j}^j) \\ \cos(\vartheta_{s_j}^j) \end{pmatrix}. \quad (3)$$

18 parameters are thus enough to parametrize all measurements appearing in the  $I_{3,3}$  expression. These can be gathered in the variable  $\vec{\alpha} = \{\vartheta_{r_j|s_j}^j, \varphi_{r_j|s_j}^j\}_{\vec{s}, j} = \{\vartheta_0^1, \vartheta_1^1, \vartheta_2^1, \vartheta_0^2, \vartheta_1^2, \vartheta_2^2, \dots, \vartheta_2^3, \varphi_0^1, \dots, \varphi_2^3\}$ . The value of  $I_{3,3}$  can then be expressed as a function of  $\vec{\alpha}$  directly, by substituting  $P(\vec{r}|\vec{s}) = \langle GHZ | M_{r_1|s_1}^1 \otimes M_{r_2|s_2}^2 \otimes M_{r_3|s_3}^3 | GHZ \rangle$  in equation (1). For instance, the probability of observing outcomes **000** when all parties use their first setting is given by

$$P(\mathbf{000}|\mathbf{000}) = \langle GHZ | M_{0|0}^1 \otimes M_{0|0}^2 \otimes M_{0|0}^3 | GHZ \rangle \quad (4)$$

After optimization of  $I_{3,3}$  over  $\vec{\alpha}$ , one finds that all values of  $\vartheta_{s_j}^j$  take the value  $\pi/2$ . This means that the settings yielding the largest value of  $I_{3,3}$  upon measurement of a GHZ state lie in the x-y plane of the Bloch sphere.